Tellus (1990), *42A*, 202–207

SHORT CONTRIBUTION

The semi-geostrophic Eady problem as a testbed for numerical simulations of frontogenesis

By HANS VOLKERT[1] and CRAIG H. BISHOP[2], [1]*Institut für Physik der Atmosphäre, DLR, D-8031 Oberpfaffenhofen, FRG;* [2]*Geophysical Fluid Dynamics Laboratory, Monash University, Clayton, Vic. 3168, Australia*

(Manuscript received 31 October 1988; in final form 16 January 1989)

ABSTRACT

The semi-geostrophic Eady problem is used as a testbed for frontogenetical calculations using a specific numerical model. Over 3 days of integration, the numerical solutions agree very well with their analytical counterparts. The increasing deviations in the vertical field of motion during the last day before the analytical model breaks down are attributed to the inability of a grid-point model to handle evergrowing contrasts correctly. The dependence of the time-scales on the external parameters is addressed.

1. Introduction

40 years ago, Eady (1949) published a paper on *Long waves and cyclone waves* in the first issue of this journal. It is now considered as a landmark contribution to dynamical meteorology in at least two ways: (i) in the original quasi-geostrophic approximation, it serves as an archetypal flow configuration which explains the baroclinic instability of a zonal shear flow; (ii) in the extended semi-geostrophic version (Hoskins and Bretherton, 1972; Hoskins, 1975), analytical solutions can be obtained which develop a frontal discontinuity within a finite time. As summarized by Reeder and Smith (1986), the view has emerged that middle latitude fronts are secondary, but nevertheless important phenomena associated with extratropical cyclogenesis.

The latter study is one among others (e.g., Keyser and Anthes, 1982; Knight and Hobbs, 1988) which use the analytical solution of the Eady problem as initial data for numerical experiments that concentrate on special aspects of frontogenesis (e.g., impact of boundary layer turbulence, comparison with observations, rôle of moisture). Although Keyser (1981) and Reeder (1985) tested their numerical control experiments against the analytical solution for an inviscid, Boussinesq flow in their Ph.D. theses, comparisons concerning the temporal evolution and the spatial structure at commensurable times cannot be found in the standard literature.

This note concentrates on the, perhaps mostly technical, issue to compare results from a particular numerical mesoscale model to analytical solutions of the Eady problem. In Section 2, the particular setting of the testbed is explained, while Section 3 is devoted to the results. Some conclusions terminate the paper.

2. The testbed

An idealized flow situation is considered as sketched in Fig. 1. The domain consists of a cross-section of length L and height H containing as basic state a uniform zonal shear flow $[\bar{u}(z) = U(z/H - 0.5)]$ relative to a steering level at $z = H/2$ with potential temperature increasing linearly with height $[\bar{\theta}(z) = \theta_0 + \Gamma(z - H/2)]$ and a constant meridional temperature gradient $[\partial\bar{\theta}/\partial y = -fU\theta_0/(gH) \equiv -\gamma]$, which is in thermal-wind

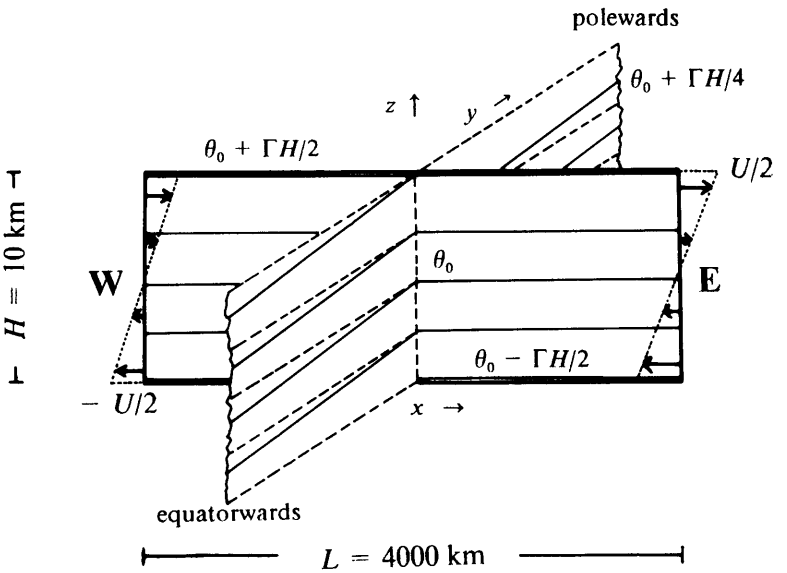

Fig. 1. Basic state of the Eady problem.

balance with the zonal shear. This basic state is a solution of the Boussinesq set of equations:

$$\rho_0 \frac{Du}{Dt} - \rho_0 fv = -\frac{\partial p}{\partial x}, \tag{1}$$

$$\rho_0 \frac{Dv}{Dt} + \rho_0 fu = -\left[\frac{\partial p}{\partial y} - \rho_0 f\bar{u}\right], \tag{2}$$

$$\rho_0 \frac{Dw}{Dt} = -\frac{\partial p}{\partial z} + \rho_0 \frac{g}{\theta_0}[\theta - \bar{\theta}] \tag{3}$$

$$\rho_0 \nabla \circ \vec{v} = 0, \tag{4}$$

$$\frac{D\theta}{Dt} = \gamma v. \tag{5}$$

In eqs. (1)–(5) u, v, w denote the full velocity components $[\bar{v} = \bar{w} = 0]$; p stands for the deviation from a hydrostatic, basic state reference pressure; the buoyancy term is expressed by deviations of potential temperature from the basic state; the forcing term in the temperature equation (5) compensates for the steady meridional heat transport. The left hand side of eq. (3) contains the non-hydrostatic contribution to the vertical motion field, which is taken into account by the numerical model (see below).

Analytical solutions for eqs. (1)–(5) can be obtained via a transformation to geostrophic coordinates, when the hydrostatic and geostrophic momentum approximations are envoked (the resulting equations are termed semi-geostrophic; cf. Hoskins, 1975). Details are given in Bishop (1989), who also treats more general basic states, e.g., by considering a combination of horizontal shear and confluence.

Solutions to the semi-geostrophic Eady problem exist only for times $t < t_\infty$,

$$t_\infty = \frac{Ls \ln\left(\frac{Lf}{2\pi v_0}\right)}{U\pi\left(\frac{2s}{\tanh(2s)} - s^2 - 1\right)^{1/2}}, \tag{6}$$

when the relative vorticity in the transformed co-ordinates equals the Coriolis parameter (f), whereas it becomes infinite in physical co-ordinates; $s = H\pi/(Lf)\cdot(g\Gamma/\theta_0)^{1/2}$ designates the growth rate parameter which equals 0.803 for the fastest growing Eady wave; v_0 is an arbitrary constant and stands for the maximum meridional wind velocity at $t = 0$. For clarity, we relabel the time axis according to

$$t^* = t - t_\infty; \tag{7}$$

the resulting negative values tell how close we are to the breakdown. The values listed in Table 1 are sufficient to obtain analytical solutions for any time $t^* < 0$ (the back-transformation onto a

specified grid in physical space is carried out numerically). Solutions at an early time are fed into the numerical model; its integration results for a later time are to be compared with the respective solution.

3. Analytical versus numerical results

The numerical experiments were carried out using the non-hydrostatic, primitive equation model *Mesoscop* (Schumann et al., 1987) in its two-dimensional, Boussinesq mode without explicit diffusion. Two program changes were necessary to sustain two-dimensional Eady wave solutions: (a) a term $\rho_0 \gamma v$ was added to the source term of the equation for the potential temperature to account for the prescribed meridional heat flux; (b) the pressure gradient in the equation for the meridional velocity v was augmented by the geostrophic contribution $-f\rho_0 \bar{u}(z)$. At the lateral boundaries, periodicity is assumed as well as rigid lids at the bottom and top ($w = 0$).

Table 1. *Independent external parameters (top) and deduced quantities (bottom) with their numerical values; see text for explanation*

Parameter	Value	
L	1000	km
H	10	km
U	40	m s^{-1}
v_0	1.5	m s^{-1}
ρ_0	0.724	kg m^{-3}
θ_0	308	K
Γ	4	K km^{-1}
γ	1.26×10^{-2}	K km^{-1}
s	0.886	
t_∞	96.6	h

The model is initialized with the basic state (cf. Fig. 1; external parameters as in Table 1) plus an incipient analytical Eady wave at $t^* = -96.6$ h and integrated over 102 h with a resolution of 81×21 gridpoints ($\Delta x = 50$ km, $\Delta z = 0.5$ km). The temporal evolution of the maxima of the meridional (v) and vertical (w) velocity components are displayed in Fig. 2 (left). The growth in v is strictly exponential

$$v_m = v_0 \exp(\alpha t); \tag{8}$$

only the growth rate ($\alpha = 1.02 \times 10^{-5}$ s^{-1}) is 5% less than the theoretical value [$\alpha_T = U\pi/(Ls)\cdot(2s/\tanh(2s) - s^2 - 1) = 1.08 \times 10^{-5}$ s^{-1}]. We note that the disturbance is not the fastest growing semi-geostrophic Eady mode, but

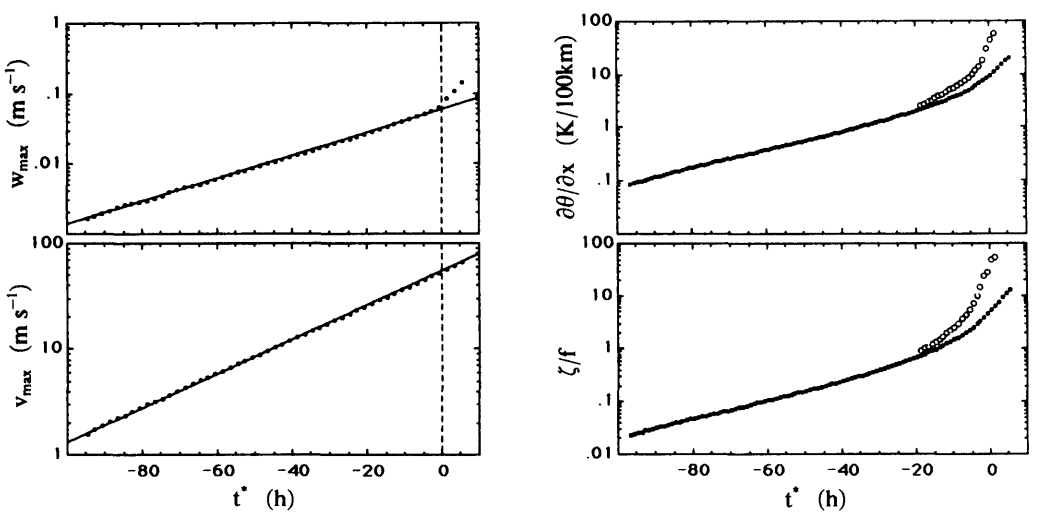

Fig. 2. Temporal evolution of various parameters. Left: maximal vertical (top) and meridional (bottom) velocity components in basic integrations. Right: surface maxima of the horizontal temperature gradient (top) and of the vorticity (normalized by the Coriolis parameter) – basic integration (dotted) and run with four-fold resolution (open circles).

reasonably close to it. The difference in growth rate is small; it is attributed to the slightly different sets of equations (there are indications that primitive equation modes grow slower than semi-geostrophic ones; Reeder, personal communication) and to inevitable deficiencies of grid-point models (e.g., implicit diffusion, analytical maximum not at grid-point etc.). The maximum in w grows exponentially as well, but with a distinct deviation at times $t^* > 0$.

The next step is to compare the spatial structure of the analytical and numerical solutions. From Fig. 2 we see that commensurable times (t_a, t_n) are those which satisfy $\exp(\alpha_T t_a = \exp(\alpha t_n)$, e.g., $t_a^* = -28.6$ h and $t_n^* = -24.6$ h (i.e., 72 h after initialization). In Fig. 3, the respective fields of vertical and meridional velocity components are juxtaposed for these times. The agreement is very satisfactory. The v field is quasi-symmetric with height (due to the constant density within the Boussinesq approximation and the rigid top and bottom boundaries). A front is developing between the southerly and northerly jets which enhance the temperature contrast by transporting warm air polewards and cold air equatorwards. The vertical motion field is upward in the warm air and downward in the cold air (direct ageostrophic circulation). As time progresses further towards t_∞, the structure of the analytical solution remains, but strengthens; the extrema in w become more displaced (maximum towards the surface front; minimum towards the (unrealistic) front at the top).

From the evidence in Figs. 2 and 3 (and other fields not displayed here), we conclude that analytical and numerical solutions agree very well, although the latter grow somewhat slower, till at least 24 h before t_∞. In order to determine whether smaller scale effects can become important at later times, a second integration with fourfold resolution (321×81 grid-points; $\Delta x = 12.5$ km, $\Delta z = 0.125$ km) is initialized at $t^* = -18.6$ h. The temporal evolution of the surface maxima of vorticity ($\zeta = \partial v/\partial x$) and the horizontal temperature gradient ($\partial\theta/\partial x$) are compared for the new and the basic run in Fig. 2

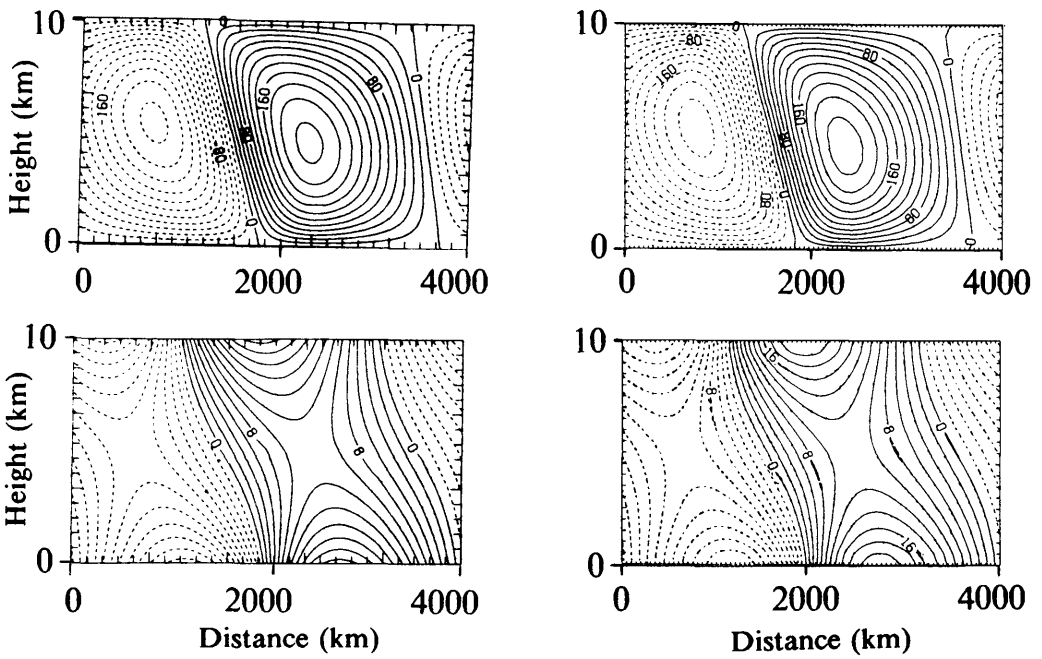

Fig. 3. Comparison between equivalent times of analytical ($t_a^* = -28.6$ h; left) and numerical solutions ($t_n^* = -24.6$ h; right): vertical (top; isoline increment: 20×10^{-4} m s^{-1}) and meridional (bottom; isoline increment: 2 m s^{-1}) velocity components; negative values dashed.

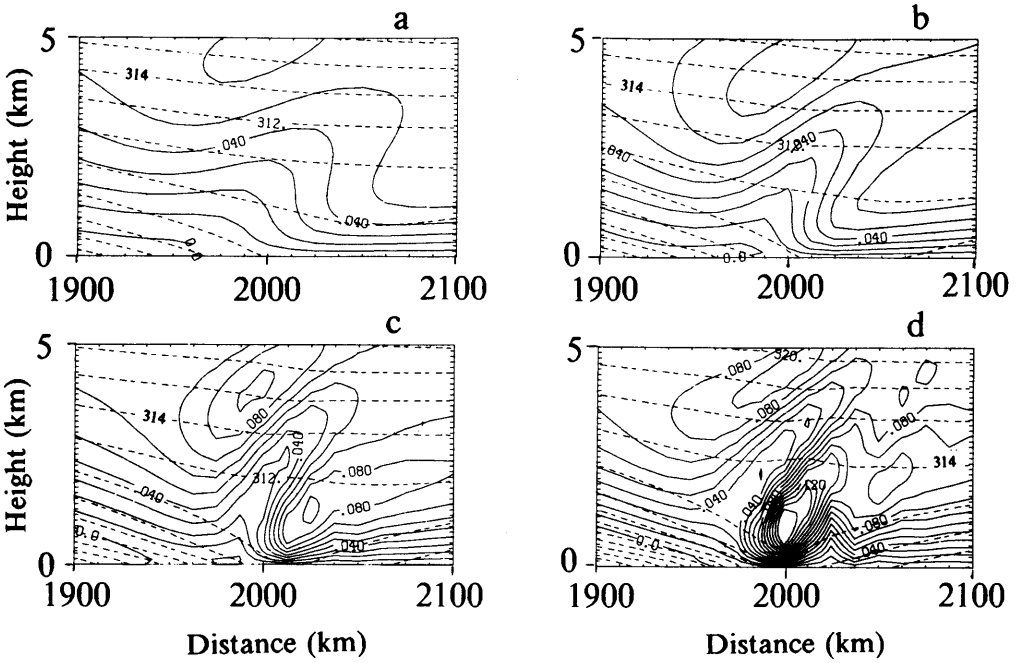

Fig. 4. Lower half of the domain's central portion with vertical velocity (full lines; isoline increment: 0.01 m s^{-1}) and potential temperature (dashed lines; isoline increment: 2 K); consecutive times: (a) $t^* = -6.6$ h; (b) $t^* = -4.6$ h; (c) $t^* = -2.6$ h; (d) $t^* = -0.6$ h) from run with four-fold resolution.

(right). The growth becomes more than exponential during the last day and it is significantly greater at four-fold resolution (in which case it started at the higher analytical level).

The vertical field of motion, as the most sensitive quantity, experiences a wave-type deviation from the analytical solution. The development of this wave (i.e., an area where the vertical velocity is reduced compared to the analytical solution) is displayed in Fig. 4 for 4 consecutive times in a blow-up of the lower part of the domain's central portion. This structure is amazingly similar to the one documented by Knight and Hobbs (1988; their Fig. 8), which they attribute to the release of conditional symmetric instability in their moist and hydrostatic calculations. A further test with resolution increased once more by a factor of 2 ($\Delta x = 6.25$ km, $\Delta z = 0.062$ km) showed very similar results, except that the tightening area of reduced vertical velocity becomes more upright (as in Knight and Hobbs, 1988; their Fig. 13).

In the present case, this feature cannot be considered physical but rather reflects the increasing inability of the grid-point model to handle the growing gradients correctly. Potential vorticity deviates from its constant, analytical value by more than 25% at some places and the vertical gradient of potential temperature becomes locally negative, which must not be the case in a flow of constant positive vorticity.

4. Conclusions

Two kinds of conclusion can be drawn. Specifically, the semi-geostrophic Eady problem was used as a very satisfactory cross-check of the independently developed analytical and numerical models. The numerical model, stripped to an idealized flow situation, followed the analytical counterpart to a degree, which, to our knowledge, was not reported before. Significant deviations from the analytical solutions became increasingly apparent during the last day before the breakdown of the analytical solution as the grid-point model could no longer correctly handle the

growing gradients. Further studies are planned to exploit more general analytical reference states relevant to frontogenesis (cf. Bishop, 1989) by a combination with numerical integrations.

More generally, the semi-geostrophic Eady problem should also be considered as a suitable testbed for numerical models dealing with frontogenesis and not only as a means to obtain a consistent initial dataset. It is useful to state how close specific calculations are to the breakdown of the analytical solution, as these become more and more unrealistic in their later stages.

REFERENCES

Bishop, C. H. 1989. *Frontogenesis and cyclogenesis.* Ph.D. thesis, Monash University, Australia.

Eady, E. T. 1949. Long waves and cyclone waves. *Tellus 1*, 33–52.

Hoskins, B. J. 1975. The geostrophic momentum approximation and the semi-geostrophic equations. *J. Atmosph. Sci. 32*, 233–242.

Hoskins, B. J. and Bretherton, F. P. 1972. Atmospheric frontogenesis models: mathematical formulation and solution. *J. Atmosph. Sci. 29*, 11–37.

Keyser, D. J. 1981. *Frontogenesis in the planetary boundary layer of an amplifying, two-dimensional baroclinic wave.* Ph.D. thesis, The Pennsylvania State University, 285 pp.

Keyser, D. J. and Anthes, R. A. 1982. The influence of planetary boundary layer physics on frontal structure in the Hoskins-Bretherton horizontal shear model. *J. Atmosph. Sci. 39*, 1783–1801.

Knight, D. J. and Hobbs, P. V. 1988. The mesoscale and microscale structure and organization of clouds and precipitation in midlatitude cyclones. Part XV: a numerical modeling study of frontogenesis and cold-frontal rainbands. *J. Atmosph. Sci. 45*, 915–930.

Reeder, M. J. 1985. *Models of frontogenesis.* Ph.D. thesis, Monash University, Australia.

Reeder, M. J. and Smith, R. K. 1986. A comparison between frontogenesis in the two-dimensional Eady model of baroclinic instability and summertime cold fronts in the Australian region. *Quart. J. R. Met. Soc. 112*, 293–313.

Schumann, U., Hauf, T., Höller, H., Schmidt, H. and Volkert, H. 1987. A mesoscale model for the simulation of turbulence, clouds and flow over mountains: Formulation and validation examples. *Beitr. Phys. Atmosph. 60*, 413–446.